Influence of projected Arctic sea ice loss on polar stratospheric ozone and circulation in spring

2014 Environ. Res. Lett. 9 084016

(http://iopscience.iop.org/1748-9326/9/8/084016)

OPEN ACCESS
IOP Publishing
Environmental Research Letters
Environ. Res. Lett. **9** (2014) 084016 (9pp)
doi:10.1088/1748-9326/9/8/084016

Influence of projected Arctic sea ice loss on polar stratospheric ozone and circulation in spring

Lantao Sun[1], Clara Deser[1], Lorenzo Polvani[2] and Robert Tomas[1]

[1] National Center for Atmospheric Research, Boulder, CO, USA
[2] Dept of Applied Physics and Applied Mathematics, and Dept of Earth and Environmental Sciences, Columbia University, New York, USA

E-mail: lantao@ucar.edu

Received 7 May 2014, revised 30 July 2014
Accepted for publication 31 July 2014
Published 26 August 2014

Abstract

The impact of projected Arctic sea ice loss on the stratosphere is investigated using the Whole Atmosphere Community Climate Model (WACCM), a state-of-the-art coupled chemistry climate model. Two 91-year simulations are conducted: one with a repeating seasonal cycle of Arctic sea ice for the late twentieth-century, taken from the fully coupled WACCM historical run; the other with Arctic sea ice for the late twenty-first century, obtained from the fully coupled WACCM RCP8.5 run. In response to Arctic sea ice loss, polar cap stratospheric ozone decreases by 13 DU (34 DU at the North Pole) in spring, confirming the results of Scinocca *et al* (2009 *Geophys. Res. Lett.* **36** L24701). The ozone loss is dynamically initiated in March by a suppression of upward-propagating planetary waves, possibly related to the destructive interference between the forced wave number 1 and its climatology. The diminished upward wave propagation, in turn, weakens the Brewer–Dobson circulation at high latitudes, strengthens the polar vortex, and cools the polar stratosphere. The ozone reduction persists until the polar vortex breaks down in late spring.

S Online supplementary data available from stacks.iop.org/erl/9/084016/mmedia

Keywords: Arctic sea ice loss, ozone, Brewer–Dobson circulation

1. Introduction

Arctic sea ice extent is declining at an accelerating pace, and climate models project a seasonally ice-free Arctic Ocean by the middle of this century in response to increasing greenhouse gas (GHG) concentrations (see Stroeve *et al* 2012, and references therein). The sea ice loss is expected to have numerous consequences for regional climates, including near-surface warming and increased precipitation at high latitudes (e.g., Screen and Simmonds 2010, Deser *et al* 2010). It is also expected to affect the large-scale tropospheric circulation, manifest as the negative phase of the Northern Annular Mode (NAM) (Thompson and Wallace 2000) in winter (see Deser *et al* 2010, Peings and Magnusdottir 2014 and references therein).

Given the projected impacts of Arctic sea ice loss on the troposphere, it is reasonable to ask whether the stratosphere might be affected as well. To our knowledge, only one study has addressed this question using a model with a well-resolved stratosphere, namely Scinocca *et al* (2009), hereafter referred to as S09. S09 examined the transient response of the fully coupled Canadian Middle Atmosphere Model to a sudden reduction in sea ice albedo and found that the polar stratosphere cools in response to Arctic sea ice loss, accompanied by a local reduction in ozone. Other studies based on 'low-top' atmospheric general circulation models without a well-represented stratosphere also find a springtime cooling of the polar stratosphere in response to present and future Arctic sea ice loss (Cai *et al* 2012, Screen *et al* 2013). In 2011,

following several years of below normal ice cover, the Arctic experienced unprecedented springtime ozone depletion, raising additional concerns about a possible linkage between Arctic sea ice loss and ozone (Manney *et al* 2011).

Building upon the results of S09, Cai *et al* (2012), and Screen *et al* (2013), we conduct experiments with the Whole Atmosphere Community Climate Model (WACCM), a state-of-the-art chemistry-climate model with a well-resolved stratosphere, to study the impact of future Arctic sea ice loss upon the stratosphere, including its circulation, temperature, and ozone concentration. Unlike S09, who studied the transient response to an abrupt idealized reduction in sea ice in a coupled model context, we here examine the steady-state atmospheric response to late twenty-first century sea ice loss projected by the fully coupled version of WACCM, driven by the RCP8.5 GHG scenario. As shown below, future Arctic sea ice loss suppresses upward-propagating planetary waves in March, resulting in a weakened Brewer–Dobson circulation at high latitudes and an associated reduction in lower stratospheric ozone, which persists until the polar vortex breaks down in late spring.

2. Model and experimental design

We use WACCM version 4, a high-top model with a horizontal resolution of 1.9° latitude and 2.5° longitude and 66 vertical levels extending from the surface to approximately 140 km. In addition to enhanced vertical resolution in the stratosphere and mesosphere, WACCM incorporates an interactive stratospheric chemistry package and special gravity wave parameterizations. These additional features make this model a better tool for studying the stratospheric response than more commonly used low-top models. Details of the model formulation and WACCM's twentieth-century transient simulation are documented in Marsh *et al* (2013).

To address the impact of future sea ice loss upon the stratosphere, we have conducted a pair of 91-year experiments. The control experiment is specified with a repeating seasonal cycle of sea ice concentration (SIC) and sea surface temperature (SST) averaged over the period 1980–1999, obtained from the average of a three-member ensemble of twentieth-century simulations with the corresponding fully coupled version of WACCM (Marsh *et al* 2013). The perturbation experiment is specified with a repeating seasonal cycle of Arctic SIC averaged over the period 2080–2099, obtained from the single available twenty-first century simulation of the fully coupled version of WACCM, forced by 'Representative Concentration Pathway (RCP) 8.5' (corresponding to a radiative forcing level of approximately 8.5 W m^{-2} by 2100). In both experiments, the radiative forcings and ozone-depleting substances (ODS) are fixed at the year 2000 so as to isolate the impact of Arctic sea ice loss. Note that we do not change SIC in the Antarctic. Following convention, sea ice thickness is specified to be 2 m in the Arctic and 1 m in the Antarctic.

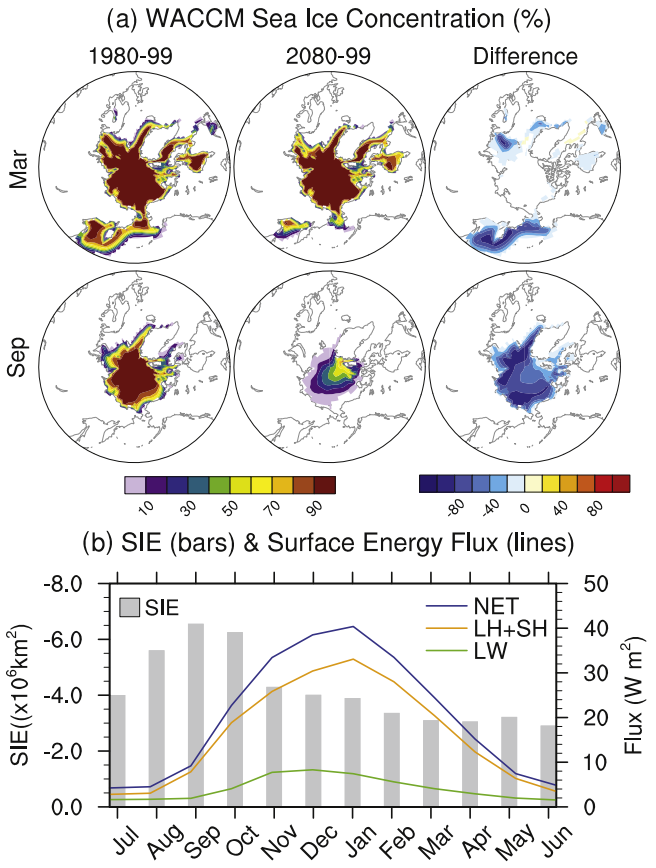

Figure 1. (a) Average Arctic sea ice concentration (SIC; %) simulated by WACCM fully coupled (left) historical simulation during 1980–1999, (middle) RCP8.5 simulation during 2080–2099, and (right) their difference (RCP8.5 minus historical) in (top) March and (bottom) September. (b) Monthly changes of Sea Ice Extent (SIE; gray bars; 10^6 km^2) between the RCP8.5 and historical simulations and the monthly responses of the net surface energy flux (blue curve), sensible plus latent heat energy flux (yellow curve), and long-wave radiative flux (green curve) averaged over the Arctic ocean (W m^{-2}, positive values upward).

The SSTs in the perturbation experiment are the same as those in the control experiment, except in areas where the fractional ice cover in the late twenty-first century is less than that in the late twentieth-century. In these cases, the SSTs are set to their 2080–2099 values from WACCM RCP8.5 run. This approach takes into account not only the sea ice loss, but also the local warming of the sea surface that occurs in association with the ice loss (see also Screen *et al* 2013). It should be noted, however, that inclusion of the local SST warming has only a small (~15%) effect on the magnitude of the Arctic Ocean's net surface heat flux response in similar experiments with Community Atmosphere Model Version 4 (CAM4) (Deser *et al* 2014). Differencing the perturbation and control experiments yields the impact of future Arctic sea ice loss and associated local SST warming on the atmosphere. A Student's t-test is used to estimate the statistical significance of the responses. We discard the first year of each 91-year simulation from our analysis.

Figure 1(a) shows the prescribed SIC distribution in March (time of maximum ice extent) and September (time of

minimum ice extent) for the control and perturbation experiments and their difference. WACCM's simulation of the present-day sea ice distribution is in good agreement with observations (e.g., Stroeve *et al* 2012), although there is some overestimation of the concentrations within the marginal ice zones. In both months, the sea ice cover contracts poleward in the late twenty-first century compared to the late twentieth-century. In March, the ice loss is limited to the marginal ice zones in the North Atlantic and Pacific. In September, however, ice loss occurs throughout the Arctic Ocean, and much of the basin is nearly ice-free by the end of the twenty-first century.

The differences in the seasonal cycles of sea ice extent (SIE) between the perturbation and control experiments are shown in figure 1(b), together with the monthly responses of the surface energy fluxes (positive upward) averaged over the Arctic Ocean. The largest ice loss between the late twentieth (1980–1999) and late twenty-first (2080–2099) centuries occurs in August–October (~6×10^6 km^2; gray bars), with a relative small seasonal dependence to the accompanying local SST increase (minimum values ~0.3°C in February–April and maximum values ~ 1.4°C in July–September; not shown). By contrast, the net surface energy flux response (blue curve) exhibits a pronounced seasonal cycle, with maximum values in winter (~40 W m^{-2} in December–January) and minimum values in summer (~5 W m^{-2} in June–August), consistent with previous studies (e.g., Deser *et al* 2010, Peings and Magnusdottir 2014). The net surface energy flux is dominated by the turbulent (sensible plus latent) component (yellow curve). Since sea ice affects the atmosphere via the surface energy fluxes, the delay between the maximum ice loss and the peak surface energy flux response has implications for the timing of the atmospheric circulation response (Deser *et al* 2010). Specifically, the impact of Arctic sea loss on the atmosphere is largest in the winter even though ice loss peaks in the fall.

3. Results

3.1. Ozone response to Arctic sea ice loss

Figure 2(a) shows the total column ozone response to projected sea ice loss as a function of latitude and month (shading), superimposed upon the control run climatology (contours). The Arctic ozone climatology in WACCM is characterized by a distinct seasonal cycle, with a maximum (~400–425 DU) in spring and a minimum (~300–325 DU) in fall, consistent with observations. In response to sea ice loss, a substantial and statistically significant polar ozone reduction is found in spring (March–April), with maximum amplitude of 34 DU at the North Pole. To illustrate the magnitude of the response relative to the internal variability, we show the records of March polar cap ozone for each year of the control and perturbation simulations (figure 2(b)). Consistent with figure 2(a), March polar ozone is reduced in most years of the perturbation experiment compared to the control experiment,

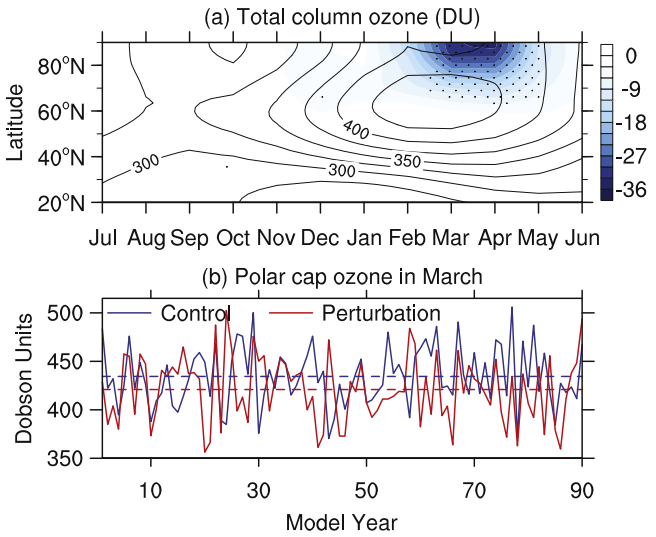

Figure 2. (a) Distribution of zonally averaged total column ozone (DU) as a function of month and latitude for the control run climatology (contours; contour interval of 25 DU) and the response to Arctic sea ice loss (shading; stippled region indicates >95% statistical significance based on a two-sided Student's t-test). (b) Time series of total column ozone (DU) averaged over the polar cap (60°N–90°N) in March from the control (blue) and perturbation (red) experiments. The horizontal dashed lines show the time-mean for each experiment.

with an overall reduction of 13 DU. However, there is large interannual variability in both experiments, with an approximate range of 150 DU. This highlights the importance of long simulations to establish the statistical significance of the response in the presence of internal variability.

3.2. Mechanism of March ozone reduction

To investigate the mechanism of the March ozone reduction, we show the responses (shading) and control run climatologies (contours) of ozone mixing ratio and residual mean circulation in figure 3(a) and (b), respectively. The residual mean circulation approximates the mean Lagrangian transport of mass through the stratosphere and is known as the Brewer–Dobson circulation (BDC). The BDC climatology is characterized by tropical upwelling and extratropical downwelling and is responsible for transporting ozone from the equatorial upper stratosphere (where ozone is produced) to the high-latitude lower stratosphere (e.g., Shepherd 2008). The circulation response to Arctic sea ice loss shows a weakening of the poleward and downwelling branches of the BDC at high latitudes. These BDC changes result in diminished transport of ozone into the polar cap in the lower stratosphere, qualitatively consistent with the reduction of the ozone mixing ratio in this region. We also analyze lower stratospheric changes in the area with a temperature below 196 K, the threshold for the formation of nitric acid trihydrate clouds (Hanson and Mauersberger 1988), and find a notable increase in response to sea ice loss. While a detailed ozone budget is beyond the scope of this short paper, this suggests

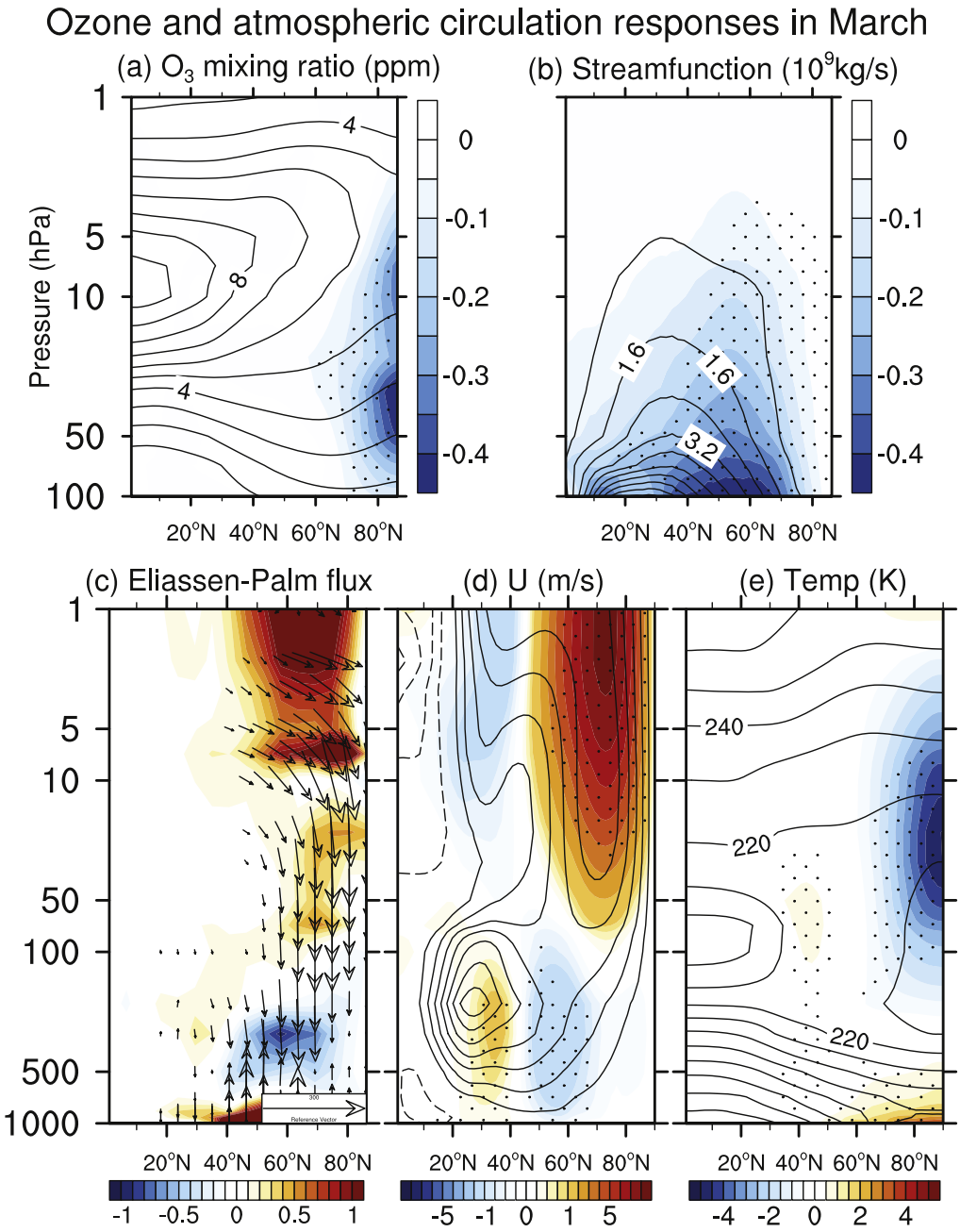

Figure 3. Distributions of March zonally averaged ozone and atmospheric circulation as a function of pressure and latitude for the control run climatology (contours) and the response to Arctic sea ice loss (shading; stippling indicates the 95% significance level). (a) Ozone mixing ratio (ppm), (b) Brewer–Dobson circulation (10^9 kg s^{-1}), (c) Eliassen–Palm (E–P) flux vector and its divergence (m s^{-1} day^{-1}; shading). Note that the climatological E–P fluxes and divergence fields are not shown. (d) Zonal wind (m s^{-1}), (e) Temperature (K). The contour intervals for ozone mixing ratio, Brewer–Dobson circulation, zonal wind, and temperature are 1 ppm, 8×10^8 kg s^{-1}, 5 m s^{-1}, and 10 K, respectively. For better display, we plot only those E–P vectors whose vertical component exceeds 10 Pa m s^{-2} in absolute value. Note that a nonlinear color scale is used for the zonal wind response (interval of 0.25 m s^{-1} for absolute value less than 1 m s^{-1} and interval of 1 m s^{-1} for absolute value larger than 1 m s^{-1}).

that both chemistry and transport play a role in the ozone loss found in our experiments.

Previous studies (e.g., Ueyama and Wallace 2010, Chen and Sun 2011, Gerber 2012) have suggested that the BDC is mainly driven by stratospheric extratropical planetary waves and gravity waves (Butchart *et al* 2010a). Therefore we examine whether the weakening of the BDC in response to sea ice loss might be related to planetary wave and/or gravity wave drivings in the stratosphere. figure 3(c) shows the response of the Eliassen–Palm vector and its divergence, a measure of resolved Rossby wave propagation and dissipation, in March. The climatology is characterized by upward wave propagation (upward Eliassen–Palm (E–P) vector) and wave dissipation (E–P convergence) in the extratropical stratosphere (not shown). In response to sea ice loss, there is a downward anomaly in the E–P vectors, indicating less

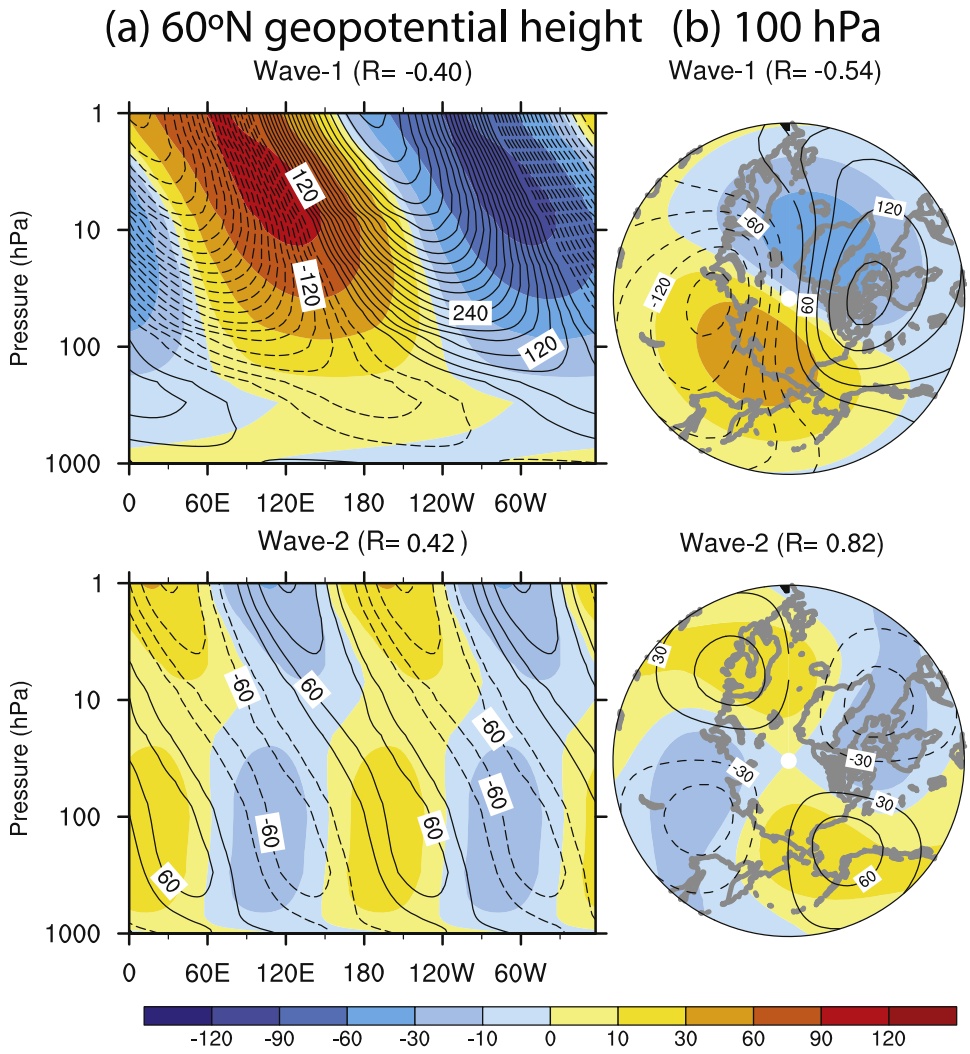

Figure 4. Forced (shading) and climatological (contour) stationary wave number (top) one and (bottom) two geopotential height fields at (a) 60°N and (b) 100 hPa in March. Results are shown as longitude-pressure (hPa) cross-sections at 60°N in the left panels and longitude-latitude maps at 100 hPa in the right panels. The contour intervals are 30 m for cross-sections at 60°N and 10 m for maps at 100 hPa. The weighted spatial correlation cofficients (R) between the contour and shading is given in each panel.

upward wave propagation into the stratosphere. Associated with this, there is reduced wave dissipation (positive E–P divergence anomaly) in the extratropical stratosphere. In order to establish the connection between changes in resolved and parameterized wave drag and the BDC more quantitatively, we use the downward control principle (Haynes *et al* 1991) to diagnose the extratropical residual streamfunction at 70 hPa associated with the stratospheric wave drag change. The results indicate that in our model almost all of the BDC reduction within the polar cap is caused by the resolved planetary waves in the stratosphere, with gravity wave drag making only a minor contribution (Supplementary Materials, available at stacks.iop.org/erl/9/084016/mmedia).

One may wonder why the upward wave propagation into the stratosphere is suppressed in March. Recent studies have suggested that forced planetary waves could interfere with the climatology so as to suppress or enhance the upward wave propagation (Garfinkel *et al* 2010, Fletcher and Kushner 2011, Smith and Kushner 2012). Figure 4 shows the forced (contour) and climatological (shading) stationary wave numbers 1 and 2 geopotential height fields at 60°N and 100 hPa in March. Both the forced and climatological wave 1 exhibit a westward tilt with height, corresponding to an upward propagating Rossby wave. At 100 hPa, the wave 1 response is largely out of phase with the control run climatology. The weighted spatial correlations at 60°N and 100 hPa are -0.40 and -0.54, respectively. This suggests that, qualitatively, the forced wave 1 is able to destructively interfere with the climatology, resulting in a suppression of upward wave propagation. In contrast, the wave 2 response is more in phase with the climatology below 10 hPa, with the weighted spatial correlations of 0.42 at 60°N and 0.82 at 100 hPa between the two fields. Therefore, wave 2 interference does not appear to explain the suppression of upward wave propagation. Further, the amplitude of the response is considerably larger for wave 1 than wave 2 (96 m compared to 7 m at 60°N and 10 hPa), another indication that wave 1 is more important than wave 2

in suppressing upward wave propagation via linear wave interference. Moreover, the E–P flux diagnostics for each wave number separately confirms that the suppression of upward wave propagation and wave dissipation in the stratosphere is indeed dominated by wave number 1 (not shown). Collectively these diagnostics point to the role of wave 1 in causing the stratospheric circulation response in March.

3.3. Zonal wind and temperature responses

The zonal-mean responses of zonal wind and temperature in March as a function of latitude and height are shown in figures 3(d) and (e), respectively. In the troposphere, the zonal wind response is characterized by a statistically significant meridional dipole in the middle latitudes, with reduced westerlies in the latitude band 45–70°N and enhanced westerlies in the band 20–40°N. This structure implies an equatorward shift of the midlatitude jet and projects onto the negative phase of the NAM, consistent with many other studies based on both comprehensive and idealized models (e.g., Deser *et al* 2010, Butler *et al* 2010, Peings and Magnusdottir 2014).

In the stratosphere, there is a marked increase of the zonal winds at high latitudes, with values exceeding 6 m s^{-1}, and a smaller amplitude reduction of the zonal winds in middle latitudes (figure 3(d)). The strengthening of the polar vortex is to be expected, given the reduced wave dissipation in the stratosphere, as the latter is responsible for decelerating the zonal wind. From the thermal wind relation, a stronger polar vortex is associated with a cooler polar lower stratosphere as seen in figure 3(e), although ozone reduction may also contribute to the cooling of the polar stratosphere as a result of diminished absorption of solar ultraviolet radiation. Near the surface, large warming in the polar region (figure 3(e)) is a result of an increase of the upward turbulent heat flux as a consequence of sea ice loss.

3.4. The role of stratospheric polar vortex final breakdown in ozone response

So far we have focused on the role of the residual circulation as a mechanism to explain the reduction of March ozone in response to projected Arctic sea ice loss. However, the mean meridional circulation is not the only way to transport ozone into the polar cap. Isentropic mixing across the vortex edge can also bring ozone-rich mid-latitude air into the polar region. This quasi-horizontal mixing weakens in response to Arctic sea ice loss due to reduced upward planetary-wave propagation and wave breaking in the stratosphere (e.g., Shepherd 2008) and may partly contribute to the polar ozone loss in March.

The timing of the breakdown of the polar vortex, also known as the stratospheric 'final warming', is an indicator of strong isentropic mixing and has been suggested to affect ozone at interannual timescales in the Northern Hemisphere (Salby and Callaghan 2007, Strahan *et al* 2013). Therefore, we examine the timing of polar vortex breakdown in both experiments. Following Black *et al* (2006), we define the onset date as the last day when the 5-day running mean zonal-mean zonal wind at 10 hPa and 70°N (jet core latitude) drops below zero without returning above 10 m s^{-1} until the following autumn. Figure 5(a) shows the time series of polar vortex breakdown dates in both experiments. The mean date in the control experiment is April 24, approximately three weeks later than in the NCEP/NCAR Reanalysis (Black *et al* 2006). This is a well-known bias of most current-generation chemistry-climate models (Butchart *et al* 2010b). In response to sea ice loss, the mean breakdown date is delayed by an average of six days (statistically significant from zero at the 97% confidence level), with the largest effect on the early side of the breakdown date distribution.

The timing of polar vortex breakdown is closely connected to the evolution of the ozone response at high latitudes. As the vortex breaks down in late April in the perturbation experiment (recall in figure 5(a) that the mean breakdown date is April 30), strong isentropic mixing brings high-ozone air from mid-latitudes into the polar region, abruptly terminating polar ozone depletion. This explains the timing of the ozone response to Arctic sea ice loss in figure 2(a), which emerges in March and persists through April until the polar vortex is finally destroyed.

To further explore how the circulation and ozone responses vary with the timing of the breakdown of the polar vortex, we select the ten earliest and ten latest vortex breakdown years from the control and perturbation experiments and construct composites for 10-hPa zonal wind and total column ozone (figures 5(b) and (c)). The polar vortex is strengthened in March for both the early and late breakdown composites in response to sea ice loss, with somewhat larger magnitude for the early breakdown years. The response in the late breakdown composite, however, persists until the middle of May, about 45 days longer than for the early breakdown composites. The ozone climatology for the early breakdown years shows larger values at high latitudes in spring than that for the late breakdown years, consistent with observations (Strahan *et al* 2013) and earlier modeling studies (Salby and Callaghan 2007). The polar ozone response to Arctic sea ice loss follows the circulation response: a larger loss for the early breakdown years that disappears quickly in April (left panel of figure 5(b)). In contrast, ozone loss for the late breakdown years is more persistent, lasting until May.

4. Summary and discussion

Our WACCM experiments, contrasting prescribed present-day and future sea ice conditions, indicate that late twenty-first century Arctic sea ice loss, if taken in isolation from other projected changes (e.g., GHGs and ODS), will induce a significant reduction in stratospheric polar ozone in association with a weakening of the BDC and a strengthening of the stratospheric polar vortex in spring. The March reduction of polar ozone in response to Arctic sea ice loss is initiated dynamically via a suppression of upward-propagating planetary waves, possibly related to the destructive interference between the forced wave number 1 and its climatology. The

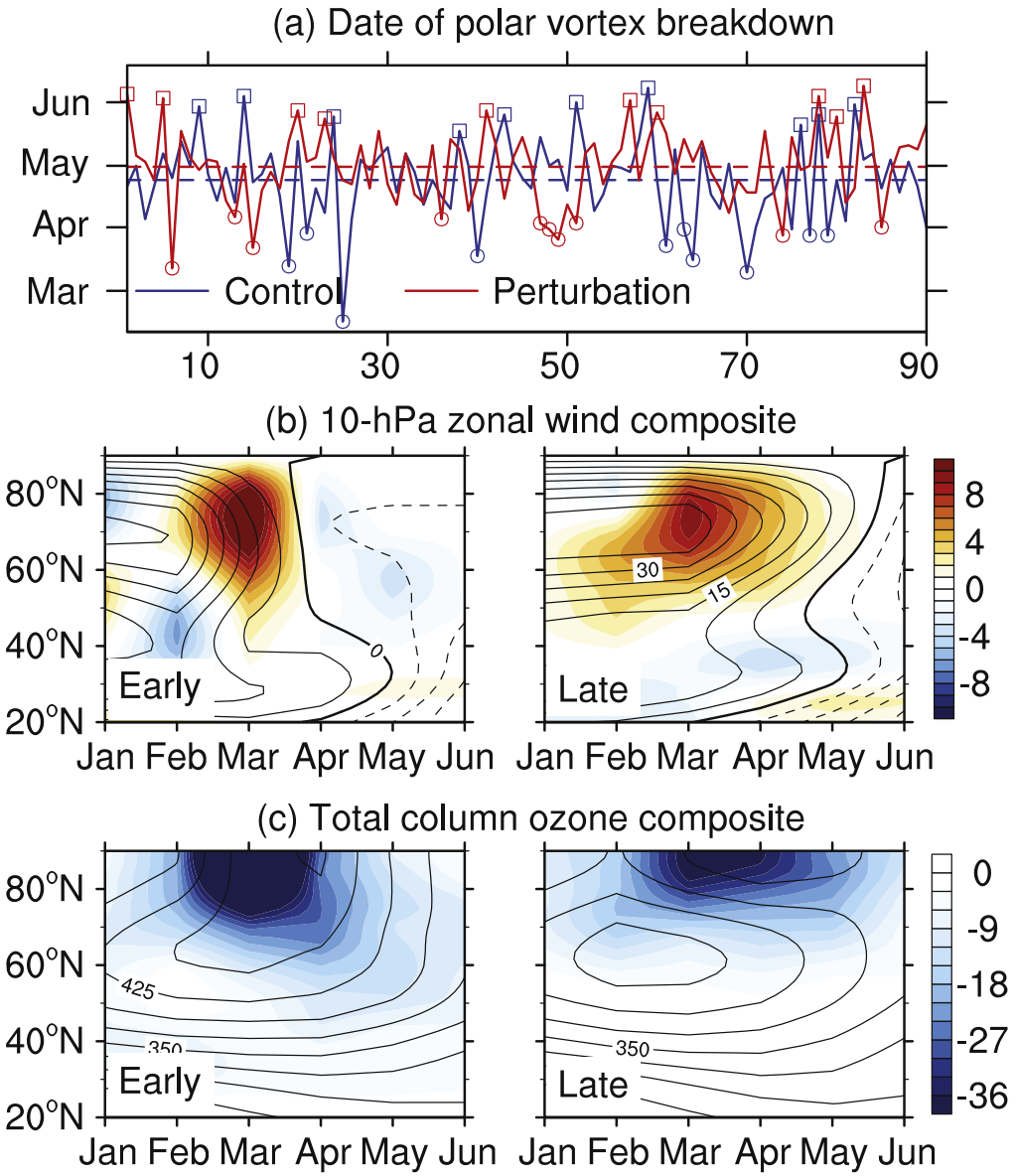

Figure 5. (a) Time series of polar vortex breakdown dates in the control (blue) and perturbation (red) experiments. Dashed lines show the mean onset dates for each experiment. Circle and rectangle markers indicate the ten earliest and ten latest polar vortex breakdown years, respectively. (b) Composites of climatological zonal wind at 10 hPa (contour) and its response to sea ice loss (shading) based on the ten earliest (denoted Early) and ten latest (denoted Late) polar vortex breakdown years. (c) As in (b), but for total column ozone. The contour intervals for zonal wind and total column ozone are 5 m s^{-1} and 25 DU, respectively.

reduced wave dissipation in the extratropical stratosphere, in turn, induces a weakening of the BDC, strengthening of the polar vortex, and cooling of the polar stratosphere. The ozone reduction persists through April until the polar vortex breaks down.

Our results are in qualitative agreement with S09, although our experimental design differs. In particular, S09 imposed a sudden reduction in sea ice albedo in their fully coupled model to represent the maximum possible forcing in which all sea ice is melted in summer, whereas we have prescribed sea ice conditions taken from WACCM's fully coupled response to historical and RCP8.5 radiative forcing to the uncoupled WACCM atmospheric model. Therefore, the magnitude of our sea ice forcing is probably more realistic in the sense that it is taken from a coupled model's simulation of future climate. In addition, the seasonality of our sea ice loss is probably more realistic than in S09 for the same reason. In particular, sea ice albedo methodology underestimates sea ice loss in winter (Deser *et al* 2014), the season in which the projected sea ice melt is expected to have the largest impact on surface energy fluxes and atmospheric circulation. Moreover, the response in S09's experiments is transient and only appears one decade after the ice albedo change is applied. In our experiments, however, since prescribed sea ice conditions are repeated for each year of the 91-year runs, we obtain the steady-state atmospheric response to sea ice loss. Despite these differences, the agreement of the response across models highlights the robustness of the results.

To further document the robustness of our results, we have conducted analogous experiments with CAM4, a 'low-top' model without interactive chemistry, with horizontal resolution of 0.9° latitude and 1.25° longitude and 26 vertical levels (eight levels above 100 hPa). The prescribed sea ice loss in the CAM4 experiments (taken from the coupled model Community Climate System Model version 4 (CCSM4)) is similar to that in WACCM (not shown). The comparison of the atmospheric circulation response to Arctic sea ice loss between WACCM and CAM4 is shown in figure S2 in the Supplementary Materials. The response in CAM4 bears a striking resemblance to the one in WACCM, including strengthening of the polar vortex and polar cap cooling in the stratosphere. However, the magnitudes are approximately 60% weaker, and the statistical significance is a little lower (around 90%) in CAM4 than in WACCM. The weaker response in CAM4 may be due to several factors, including differences in model physics, the lack of interactive stratospheric chemistry, and the lack of a well-resolved stratosphere. We note that the climatological polar vortex is much stronger in CAM4 than in WACCM (maximum zonal-mean zonal wind at 10 hPa and 70°N is 45 m s^{-1} in CAM4 compared to 25 m s^{-1} in WACCM, likely due to the absence of stratospheric sudden warmings in CAM4), a factor which might also affect the response to sea ice forcing (e.g., Peings and Magnusdottir 2014). Nevertheless, the qualitative resemblance between the responses in CAM4 and WACCM adds robustness to the findings reported here.

It should be noted that the March zonal wind changes caused by the loss of Arctic ice have opposite signs across the tropopause, with a negative NAM response in the troposphere (i.e., an equatorward shift of the eddy-driven jet) accompanying a positive NAM response in the stratosphere (i.e., a stronger polar vortex). This is in contrast to the zonal wind changes in winter, which show negative NAM responses in both the troposphere and stratosphere (i.e., an equatorward shift of the eddy-driven jet with a weakened polar vortex; not shown). The winter response more closely resembles the typical pattern of stratosphere-troposphere coupling in which NAM anomalies have the same sign across the tropopause (e.g., Gerber and Polvani 2009). The dynamical mechanisms behind the different vertical structures of the circulation responses in winter and spring warrant further investigation.

Finally, we note that in our experiments there is a substantial reduction of polar ozone in both March and April (13 and 14 DU, respectively) in response to Arctic sea ice loss. Given that ozone recovery proceeds at an approximately linear pace of 11 DU $decade^{-1}$ in the fully coupled WACCM RCP8.5 simulation (not shown), this means that Arctic sea ice loss acts to delay ozone recovery by approximately 12 years, similar to the delay estimated in S09. However, since the Northern Hemisphere polar ozone is expected to recover by the middle of this century (earlier than the future sea ice forcing used here), this delay time is likely to be an upper bound.

Acknowledgments

The authors would like to thank Drs. Walter Robinson, Paul Kushner, Gang Chen, and Yaga Richter for valuable discussions, and Adam Phillips for help with NCL graphics. We also appreciate the constructive comments from three anonymous reviewers. This study is supported by the National Science Foundation (NSF) Arctic System Science Program. NCAR is sponsored by the NSF. The work of LMP is funded, in part, by a grant from the NSF.

References

Black R X, McDaniel B A and Robinson W A 2006 Stratosphere-troposphere coupling during spring onset *J. Clim.* **19** 4891–901

Butchart N *et al* 2010a Chemistry-climate model simulations of twenty-first century stratospheric climate and circulation changes *J. Clim.* **23** 5349–74

Butchart N *et al* 2010b in *SPARC report on the evaluation of chemistry-climate models* ed V Eyring, T G Shepherd, D W Waugh SPARC Report No. 5, WCRP-132, WMO/TD-1526

Butler A H, Thompson D W J and Heikes R 2010 The steady-state atmospheric circulation response to climate change-like thermal forcings in a simple general circulation model *J. Clim.* **23** 3474–96

Cai D, Dameris M, Garny H and Runde T 2012 Implications of all season Arctic sea ice anomalies on the stratosphere *Atmos. Chem. Phys.* **12** 11819–31

Chen G and Sun L 2011 Mechanisms of the tropical upwelling branch of the Brewer–Dobson circulation: the role of extratropical waves *J. Atmos. Sci.* **68** 2878–92

Deser C, Tomas R and Sun L 2014 The role of ocean-atmosphere coupling in the zonal-mean atmospheric response to Arctic sea ice loss *J. Clim.* submitted

Deser C, Tomas R A, Alexander M A and Lawrence D 2010 The seasonal atmospheric response to projected Arctic sea ice loss in the late twenty-first century *J. Clim.* **23** 333–51

Fletcher C G and Kushner P J 2011 The role of linear interference in the annular mode response to tropical SST forcing *J. Clim.* **24** 778

Garfinkel C I, Hartmann D L and Sassi F 2010 Tropospheric precursors of anomalous northern hemisphere stratospheric polar vortices *J. Clim.* **23** 3282

Gerber E P 2012 Stratospheric versus tropospheric control of the strength and structure of the Brewer–Dobson circulation *J. Atmos. Sci.* **69** 2857–77

Gerber E P and Polvani L M 2009 Stratosphere-troposphere coupling in a relatively simple AGCM: the importance of stratospheric variability *J. Clim.* **22** 1920–33

Hanson D and Mauersberger K 1988 Laboratory studies of the nitric acid trihydrate: implications for the south polar stratosphere *Geophys. Res. Lett.* **15** 855–8

Haynes P H, Mcintyre M E, Shepherd T G, Marks C J and Shine K P 1991 On the 'downward control' of extratropical diabatic circulations by eddy-induced mean zonal forces. *J. Atmos. Sci.* **48** 651–78

Manney G L *et al* 2011 Unprecedented Arctic ozone loss in 2011 *Nat. Geosci.* **478** 469–75

Marsh D R, Mills M J, Kinnison D E, Lamarque J-F, Calvo N and Polvani L M 2013 Climate change from 1850 to 2005 simulated in CESM1(WACCM) *J. Clim.* **26** 7372–91

Peings Y and Magnusdottir G 2014 Response of the Northern Hemisphere atmospheric circulation to current and projected Arctic sea ice decline : a numerical study with CAM5 *J. Clim.* **27** 244–64

Salby M L and Callaghan P F 2007 Influence of planetary wave activity on the stratospheric final warming and spring ozone *J. Geophys. Res.* **112** 20111

Scinocca J F, Reader M C, Plummer D A, Sigmond M, Kushner P J, Shepherd T G and Ravishankara A R 2009 Impact of sudden Arctic sea ice loss on stratospheric polar ozone recovery *Geophys. Res. Lett.* **36** L24701

Screen J a and Simmonds I 2010 The central role of diminishing sea ice in recent Arctic temperature amplification *Nature* **464** 1334–7

Screen J A, Simmonds I, Deser C and Tomas R A 2013 The atmospheric response to three decades of observed arctic sea ice loss *J. Clim.* **26** 1230–48

Shepherd T G 2008 Dynamics, stratospheric ozone, and climate change *Atmos. Ocean* **46** 117–38

Smith K L and Kushner P J 2012 Linear interference and the initiation of extratropical stratosphere-troposphere interactions *J. Geophys. Res.* **117** D13107

Strahan S E, Douglass A R and Newman P A 2013 The contributions of chemistry and transport to low arctic ozone in march 2011 derived from Aura MLS observations *J. Geophys. Res.: Atmos.* **118** 1563–76

Stroeve J C, Kattsov V, Barrett A, Serreze M, Pavlova T, Holland M and Meier W N 2012 Trends in Arctic sea ice extent from CMIP5, CMIP3 and observations *Geophys. Res. Lett.* **39** L165020

Stroeve J C, Serreze M C, Holland M M, Kay J E, Malanik J and Barrett A P 2012 b: The Arctic rapidly shrinking sea ice cover: a research synthesis *Clim. Change* **110** 1005–27

Thompson D W J and Wallace J M 2000 Annular modes in the extratropical circulation. Part I: month-to-month variability *J. Clim.* **13** 1000–16

Ueyama R and Wallace J M 2010 To what extent does high-latitude wave forcing drive tropical upwelling in the Brewer–Dobson circulation? *J. Atmos. Sci.* **67** 1232–46